Development and Validation of an MRI-Based Method for Particle Concentration Measurement

Daniel D. Borup*

Department of Mechanical Engineering
Stanford University
488 Escondido Mall
Stanford, California 94305
borup@stanford.edu

Chris J. Elkins

Department of Mechanical Engineering
Stanford University
488 Escondido Mall
Stanford, California 94305

John K. Eaton

Department of Mechanical Engineering
Stanford University
488 Escondido Mall
Stanford, California 94305

ABSTRACT

Dilute, dispersed multiphase flows are of critical importance in engineered, environmental, and biological applications. Traditional laser-based techniques are limited to data acquisition in discrete 2D planes with optical access required. Magnetic Resonance Imaging (MRI) is finding increasing use as a diagnostic for 3D measurements in complex turbulent flows where no optical access is possible. A new diagnostic called Magnetic Resonance Particles (MRP) has been developed whereby the volume fraction of dispersed microparticles in water can be measured quantitatively. Data obtained for dilute loadings of bismuth, graphite, and titanium powder suspended in agar gel showed excellent agreement with theoretical predictions from the MRI literature. The spatial extent of signal disturbance was investigated using an individual stainless steel particle suspended in gel. Finally, a full-scale experiment was performed in which a streak of titanium particles was injected into a complex, turbulent channel flow. Calibration values were obtained using an integral flux method and the resulting particle concentration distribution was analyzed. The calibration values showed some disagreement with theory; this issue will be the focus of upcoming calibration experiments in a channel flow with homogeneous particle distribution.

INTRODUCTION

Dilute, dispersed multiphase flows are of interest in a wide range of applications including dust ingestion in aircraft engines, medicinal inhalants in the human airways, and sedimentary transport in coastal ecosystems. In commercial aircraft, the introduction of atmospheric dust can shorten engine service life significantly (Dunn *et al.*, 1987), while volcanic ash can cause near-instantaneous engine failure (Dunn, 2012). Improved knowledge of, and prediction capabilities for particle transport characteristics in a turbine engine's various subsystems would lead to improved efficiency in a major global industry. When inhaled by humans, particulate matter can be either beneficial (e.g., medicines) or harmful (e.g., airborne pollutants), but in either case it is useful to know where the particles are likely to flow and accumulate. A comprehensive review of particle transport in the human airways was provided by Kleinstreuer & Zhang (2010).

Despite the wealth of applications in which detailed particle flow quantification would be beneficial, there are significant limitations on the collection of particle concentration data using currently available techniques. Such techniques are almost entirely based on optical methods in which data are acquired in distinct 2D planes through the use of a laser sheet and camera. This 2D acquisition limits the rate at which data can be obtained. Moreover, allowing undistorted optical access for the laser-camera pair imposes severe restrictions on the complexity of the geometry that can be studied. While 3D data sets can be amassed as a stack of 2D planes, the time, cost, and complexity of compiling such data sets is quite high. Given the scarcity of fully 3D data sets in the literature, it may be concluded that these concerns are rather prohibitive.

Magnetic Resonance Imaging (MRI) is becoming an increasingly widespread tool for fundamental study of fluid mechanics and model validation in complex turbulent flows. Two diagnostics making use of a standard medical-grade MRI scanner are currently available. The first, known as Magnetic Resonance Velocimetry (MRV) allows 3D measurement of the 3-component velocity field (Elkins & Alley, 2007), while the second, known as MRC, is used to measure the 3D scalar concentration field in two-stream mixing studies (Benson *et al.*, 2010). Both techniques are becoming increasingly popular because they are much more efficient than other 3D measurements—data sets comprising several million points can be acquired over a roughly 12 hour period—and because they permit the use of geometrically complex 3D-printed models. Recent studies highlighting these capabilities include flow in a coral colony (Chang *et al.*, 2009), flow through a series of porous fins (Coletti *et al.*, 2014*b*), and flow through a patient-specific human lung model (Banko *et al.*, 2015).

An early proof-of-concept study which included qualitative MRI measurements of a streak of glass particles in a turbulent pipe flow was performed by Coletti *et al.* (2014*a*). The objective of this paper is to present development and validation details for a new MRI-based method known as Magnetic Resonance Particles (MRP) that will enable researchers to quickly and *quantitatively* measure the 3D, time-averaged particle concentration distribution. The combination of 3D velocity data with the 3D particle concentration field obtained using MRP will provide a means to advance our funda-

*Contact Author

mental knowledge and modeling capabilities in the bevy of complex systems where dilute, dispersed multiphase flows are of interest.

MRP METHOD DETAILS

Theory

Magnetic Resonsance Imaging makes use of the tendency for charged atomic nuclei (e.g., the proton nucleus of a hydrogen atom) to precess around an applied magnetic field. The rate of precession is known as the Larmor frequency and is governed by the field strength, B_0, and a parameter known as the gyromagnetic ratio, γ, according to the relationship

$$\omega = \gamma B_0 \tag{1}$$

Typical full body medical MRI scanners use 1.5 or 3 Tesla primary magnets. For all experiments described in this paper, a 3T medical-grade MRI machine was used (GE Healthcare).

Water protons entering the magnet bore initially align themselves with the main magnetic field. To produce an MRI image, a sequence of "excitiation and acquisiton" is repeated wherein the proton alignment is rotated transverse to the main field (excitation) and the induced field from the precessing protons is measured by an electromagnetic coil (acquisition). Linear magnetic field gradients applied in the three Cartesian directions change the local resonance frequency, allowing positional information to be encoded in the signal phase. Were these the only effects, the MRI signal would otherwise remain constant in time. However, thermal motion of the molecules and other perturbations to the magnetic field cause the signal to decay during the period of time between excitation and acquisition. A user-controlled parameter known as the "echo time", or TE, sets the length of this delay. When using a Gradient-Recalled Echo (GRE) sequence—the basis for MRV and MRC measurements in turbulent flows—the decay rate is deonted R_2^* ("R Two Star"), which has dimensions of inverse time.

Small paramagnetic or diamagnetic microparticles dispersed in water increase the signal decay rate by locally disturbing the magnetic field. Yablonskiy & Haacke (1994) considered this effect in the so called "static dephasing" regime, which refers to a size range of objects for which the water self-diffusion length scale is much smaller than the object size. In the presence of randomly distributed spheres, R_2^* is increased by the following additive factor, adapted from Eqn. 11 of Yablonskiy & Haacke (1994):

$$R^*_{2,part} = A\phi_v = \frac{8\pi^2}{9\sqrt{3}}\gamma B_0 |\Delta\chi|\phi_v \tag{2}$$

where A is a convienent symbol that will be referred to as the "calibration constant" and $\Delta\chi$ is the dimensionless magnetic susceptibility difference between the particle and surrounding fluid, expressed in Electromagnetic Units (EMU). This linear relationship between signal decay rate and particle volume fraction is the basis of the MRP method.

In addition, it will be important to consider the spatial extent of signal decay induced by any *one* particle alone. At any point in the fluid we can describe our position relative to the particle center in polar coordinates, (r,θ,ϕ), where θ is the polar angle from the B_0 direction axis. Using these coordinates we can define a dimensionless "dephasing position" u_p:

$$u_p = \frac{\rho}{d_p}\left[\frac{16}{3}\gamma B_0 |\Delta\chi|(TE)\right]^{-1/3} \tag{3}$$

where d_p is the particle diameter and ρ is the "equivalent polar radius" given by

$$\rho = r\left|\frac{3\cos^2(\theta)-1}{2}\right|^{-1/3} \tag{4}$$

The ratio of disturbed to undisturbed signal at any point near the single particle depends only on the dephasing position:

$$\frac{S}{S_0} = \cos\left(\frac{\pi}{2u_p^3}\right) \tag{5}$$

As expected, the signal returns to its undisturbed value as u_p increases. For $u_p > 1.7$ the signal can be considered "undisturbed" as $S/S_0 > 95\%$ when this criterion is satisfied. Equation 3 indicates that the spatial extent of signal dephasing increases with both TE and $|\Delta\chi|$. In addition, Eqn. 4 shows that for a given u_p the largest r corresponds to $\theta = 0$ or π. In other words, out of all the physical locations described by a given amount of signal loss, the ones farthest from the particle center are located along the axis of the B_0 field. The distance is only 20% smaller at $\theta = \pi/2$.

Data Acquisition

A GRE sequence developed at Stanford University and known as "mFast" was used for all MRP measurements. Within mFast, the scan operator can specify a set of TEs to be sampled. It is important to recognize that MRI does not make a series of pointwise measurements in the flow; instead, each measurement in MRI is a value of the spatial Fourier transform of the signal. For a given set of echo times, each TE is sampled in a separate excitation/acquisition pair at one point in Fourier space. After a full 2D or 3D data set has been obtained, the inverse Fourier transform is used to convert the raw data into to physical space data. When making measurements in the presence of turbulence, significant noise results from the chaotic nature of the flow. Noise reduction is achieved through multiple-scan averaging. The number of scans is referred to as the "NEX" and typically falls in the range of 12 to 16, with the signal-to-noise ratio (SNR) generally increasing with $\sqrt{NEX}$.

EXPERIMENTAL CONFIGURATION

Gel Suspensions

MRI measurements were obtained inside small glass vials containing titanium microspheres suspended in an agarose gel matrix of water and dissolved copper sulfate. The particles were grade 23 titanium alloy ($\rho = 4.43$ kg/m^3) acquired from LPW Technologies. The nominal diamter was 15–45 microns, while Gu *et al.* (2014) reported a mean and standard deviation of 33 ± 9 μm for similar (grade 5) titanium powder from LPW. The gel suspensions were prepared by dissolving agarose powder (ThermoFischer Scientific) into 0.01 M copper sulfate solution, at a ratio of 2% by mass, after the solution had been brought to boil in a microwave. Immediately after the agarose was fully dissolved, approximately 30 mL was poured into a vial and a known mass of the titanium particles was added. The vial was agitated by repeated inversion to prevent particles settling and accumulating at the bottom. Agitation was halted just before the gel solidifed to allow some time for any bubbles to escape. A similar procedure was used to produce gel suspensions of 50 micron glass microspheres (Potters Industries) as well as -200 mesh ($< 75\mu$m) bismuth and graphite powders (ThermoFischer Scientific).

An additional experiment was performed in which a single stainless steel microsphere (type 304, LPW Technologies) was

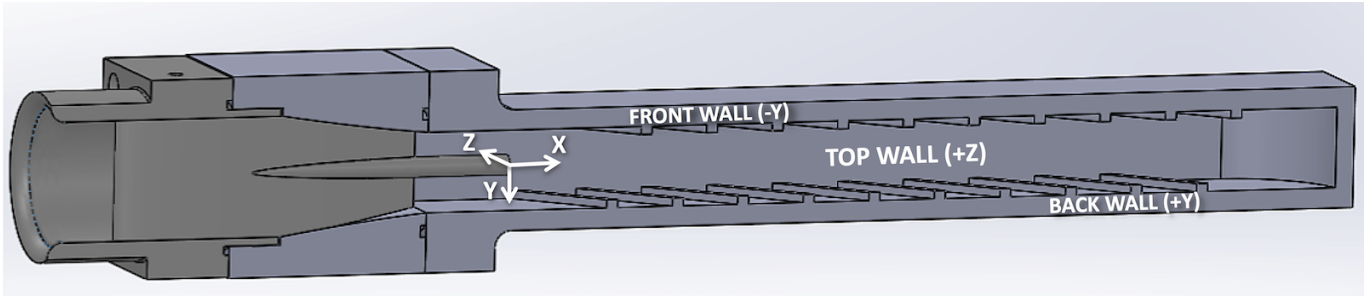

Figure 1. Cut section rendering of first passage as viewed through removed bottom wall ($-Z$).

placed in an otherwise clean gel sample. This was accomplished by preparing a clean gel vial as above and placing the lower half of the vial into an ice bath until solidified. A single particle was identified from a powder sample, measured with a jeweler's microscope, lifted by electrostatic adhesion to a needle, and released into the vial where it settled to the surface of the solidified section. After the remainder of the agar gel was allowed to congeal, the location of the particle was identified and marked on the vial exterior to aid in imaging.

Particle Streak

A full-scale test of MRP was performed by measuring particle concentration for a streak of particles injected into the center of a complex turbulent channel flow. The geometry of the flow is known as the Stanford Generic Turbine Internal Passage (SGTIP) and has been the focus of several studies dating back to Elkins *et al.* (2004). The SGTIP consists of a four-passage serpentine square channel of height $H = 20mm$. In each passage, the two walls running parallel to the plane of the serpentine's bends contain 10 rows of ribs (height $h_{rib} = 2mm$) oriented at 45° to the main flow direction. These rows are staggered on the opposing walls with each wall having an inter-rib spacing of $5h_{rib}$. Particle streak injection was performed using a 3.5-mm ID tube protruding from the back of an airfoil, shown via cut section along with the first passage of the SGTIP in Fig. 1. The coordinate origin is taken to be at the center of the injector exit. Three-dimensional mean velocity data with a particle-free streak, obtained using MRV, are omitted here for brevity but reported in Coletti *et al.* (2014*a*).

The main stream and particle streak velocities were matched to produce a bulk velocity $U_{bulk} = 1$ m/s and Reynolds number $Re = 20,000$. Particles were injected at a concentration $\phi_v = 1\%$ by volume. The main flow was supplied by a 1/3 horsepower pump (Little Giant #TE-5.5-MD-SC-HC) and controlled via a diaphragm valve. Clean flow to the streak was supplied from the same reservoir via 1/12 horsepower centrifugal pump (Little Giant #3-MD-SC) metered through a needle valve. Heavily particle-laden solution for the particle streak was supplied from an in-house designed and fabricated, MRI-compatible feeder consisting of a 20 L acrylic cylinder, rotated at 30 RPM to continuously suspend the particles. The cylinder is internally divided into two compartments by a rubber bellows; the outer compartment contains the mixture of particles and fluid, while the inner compartment is filled with water during an experiment, displacing an identical quantity of particle solution without diluting the mixture. Supply to the feeder was provided by a submersible pump (Little Giant #3E-12N) and controlled with a needle valve. Both streak supply lines were monitored using ultrasonic flow probes (Transonic Systems), while the main flow was measured using a paddlewheel flowmeter.

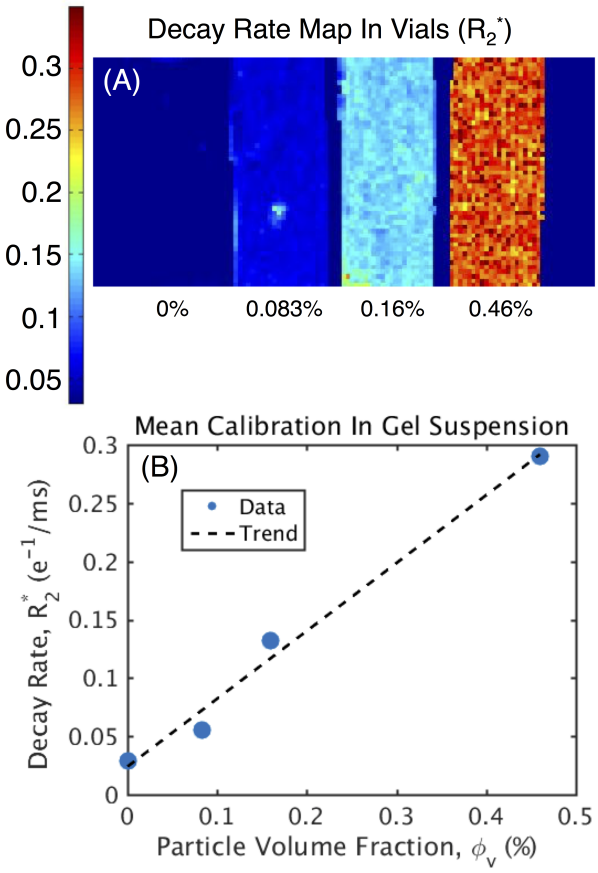

Figure 2. Particle calibration in gel suspensions. (A) Signal decay rate map in four vials. (B) Mean signal decay rate vs. mean particle concentration.

RESULTS & DISCUSSION

Gel Suspensions

Taking the 33-micron diameter titanium as an example case, four vials were prepared with mean dispersed phase volume fractions of 0%, 0.083%, 0.16%, and 0.46%. Data were obtained for all four vials simultaneously in 3D as well as in a 2D plane passing through the center of the vials. Signal magnitude was measured at several echo times ranging from 2 to 20 milliseconds in order to map the signal decay rate. Several sets of echo times were tested, but the choice of echo times did not appreciably affect the calibration constant A. Figure 2A shows a spatial map of decay rate in the four vials, while Fig. 2B reports the mean calibration in the same vials based on four echoes (2, 5, 10, and 20 ms). Some nonlin-

earity is present in the calibration due to inhomogeneity in the gel suspensions and measurement noise. The overall trend, however, is linear with a slope of 0.594 exponential decays per millisecond per percent titanium by volume; this will be reported more concisely throughout the paper as a calibration constant $A = 59.4$ kHz.

Bismuth, graphite, and glass powder gel suspensions were examined in the same manner using data at the same set of echo times. A complete list of predicted and measured calibration constants is included in Table 1[1]. It should be noted that the range of sampleable TEs is limited to around 2–20 ms by the requirements of the mFast sequence and the need for relatively short scan times. This limiatation, in combination with Eqn. 2, sets a loose upper bound on measureable ϕ_v; larger concentrations will cause the signal to die out completely before any data can be collected, leaving nothing with which to determine R_2^*. The end result is that particles with higher $|\Delta\chi|$ can be imaged at lower concentrations. The second column of Table 1 indicates the ϕ_v range of samples prepared, giving an idea of the measureable range for each material.

Table 1. Calibration constants for four particle materials.

		$\Delta\chi$ (EMU)	A (kHz)	
Material	ϕ_v (%)	$x10^6$	Predicted	Measured
Glass	0–4	-0.388	1.57	3.5
Bismuth	0–0.34	-12.3	50.0	44
Graphite	0–0.29	-15.5	63.0	63
Titanium	0–0.46	+15.2	61.8	59

Agreement between the measured and predicted calibration constant, A, is seen to improve with increasing $|\Delta\chi|$. Equation 2 only considers the space occupied by a spherical particle and the distortion to a uniform magnetic field surrounding it; at low susceptibility and high concentration, the role of particle shape, interface effects, or distortion of excitation/acquisition signal may be playing a more significant role in the signal decay process. Because MRP is intended for the study of *dilute* particle-laden flows, the use of a higher-susceptibility element is clearly preferable.

Figure 3 shows one slice of 3D signal magnitude data taken at TE = 10 ms in the neighborhood of a single, 105 μm diameter stainless steel particle. The magnetic susceptibility of stainless steel is approximately 500×10^{-6} (in EMU). The data set was obtained on a $1mm^3$ grid, so the particle diameter is 10.5% the grid spacing. While only the center voxel contains the particle, it is clear the signal decay extends to neighboring voxels on all four sides of the particles. Examination of the adjacent 2D slices shows that the signal decay extends out of plane, as well. By applying the particle properties to Eqns. 3–5 we observe that the minimum "undisturbed radius" is around 1.5 mm along the B_0 axis (up/down, in Fig. 3) and 1.2 mm in the transverse plane. While the location of one isolated particle can easily be resolved to sub-voxel resolution, doing so for an arbitrary suspension of many particles would be prohibitive. So, although a dispersed phase of higher magnetic susceptibility can be detected at lower loadings, particles of sufficient size and susceptibility will compromise the spatial resolution of the measurement.

[1] All $|\Delta\chi|$ values taken from Schenck (1996).

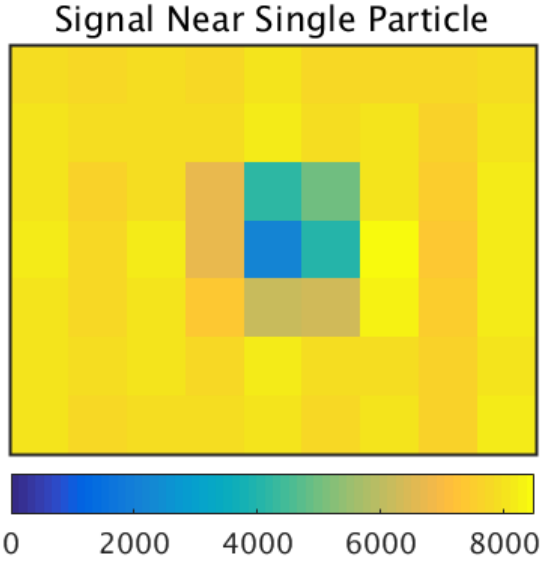

Figure 3. Signal magnitude at TE = 10 ms near a single, 105-μm diameter stainless steel particle.

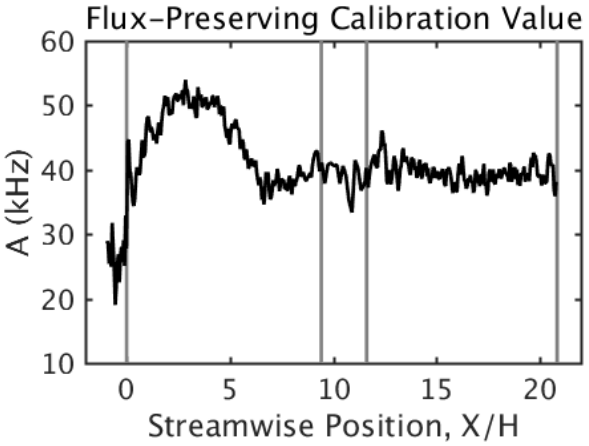

Figure 4. The required value of A to reproduce the actual particle flux. Vertical lines mark the start/end of the first two passages.

Particle Streak

The streak experiment represents the first use of MRP to measure particle concentration quantitatively in a turbulent flow. Because the exact ϕ_v distrubtion was not known a priori, it was not possible to compute the calibration constant A in a pointwise manner. However, because the inlet flow rates and concentrations were measured during the experiment and no particles were accumulating in the model, the actual particle mass flux through the SGTIP was known to be 0.43 grams per second. To determine the correct calibration value, flux was also computed for streamwise planes of data by integrating the combined MRV and MRP data. Figure 4 shows the value of A required at each streamwise position to produce the correct particle flux. It is evident that these values differ from the calibration suggested by both the theory and gel vial data. The closest agreement to theory was obtained approximately 3 channel heights after injection, where the required A was 15% too low (52 kHz). Over the bulk of the channel the required A was ~36% too low (39 kHz). For the purpose of producing a physically reasonable particle concentration field, the locally correct value of

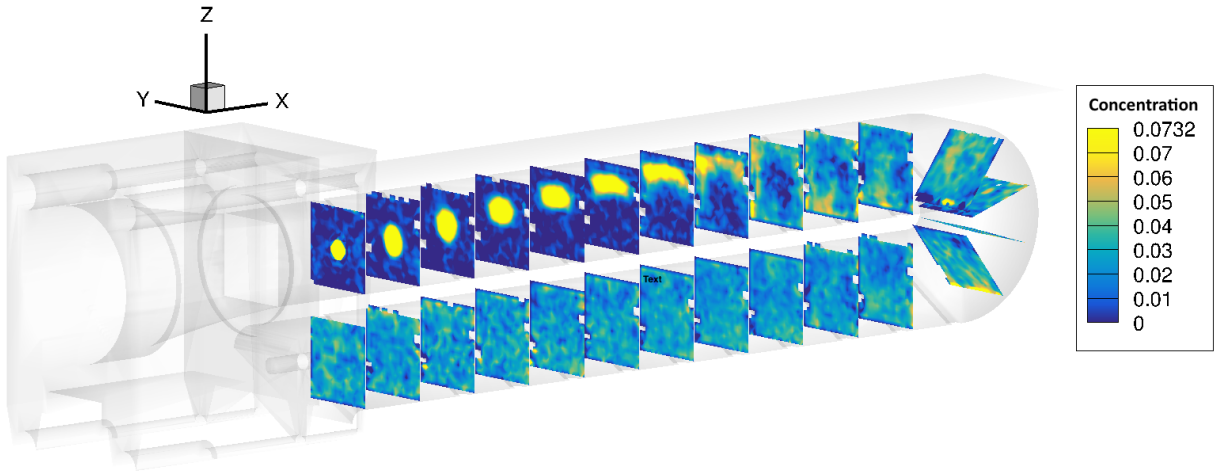

Figure 5. Particle concentration in first two passages of channel.

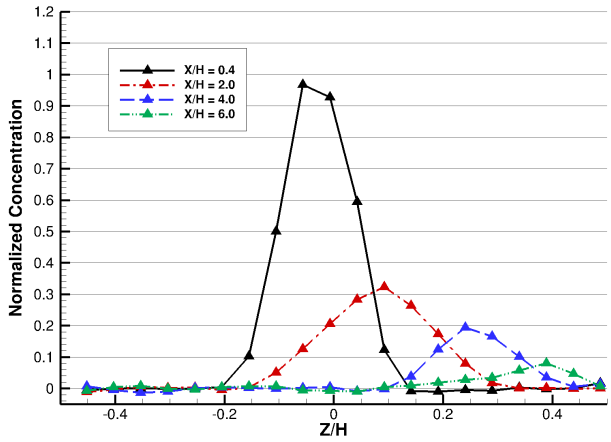

Figure 6. Concentration profiles in the Z direction at $Y = 0$ for four streamwise locations.

A was applied to compute $\phi_v(x,y,z)$; the discrepancy with theory and static data will be discussed further in the following section.

Figure 5 shows color contours of the particle streak in the first two passages of the four-passage serpentine, highlighting the fully 3D nature of the data. The streak is injected at the upper left. Flow proceeds from left to right in the upper passage and from right to left in the lower. The high-concentration, highly coherent streak is visible through the first half of the first passage as it is carried towards the top ($+Z$) wall due to strong secondary flows induced by the channel ribs. Approaching the end of the first passage, particles are dispersed along all four channel walls, leaving a low concentration region at the center. The particle concentration is essentially uniform upon exiting the bend, and remains that way throughout the second passage.

Figure 6 shows Z-direction profiles of particle concentration in the $Y = 0$ centerplane at streamwise positions $X/H = 0.4$, 2, 4, and 6. The first profile shows that just after injection the particles are narrowly distributed in the center of the channel. By $X/H = 2$ turbulent dispersion has acted to double the width of the streak and reduced peak concentrations to a third of their original value. Peak concentration continues to drop to 0.2% and 0.1% in the last two profiles, while the streak narrows as it impinges on the top wall.

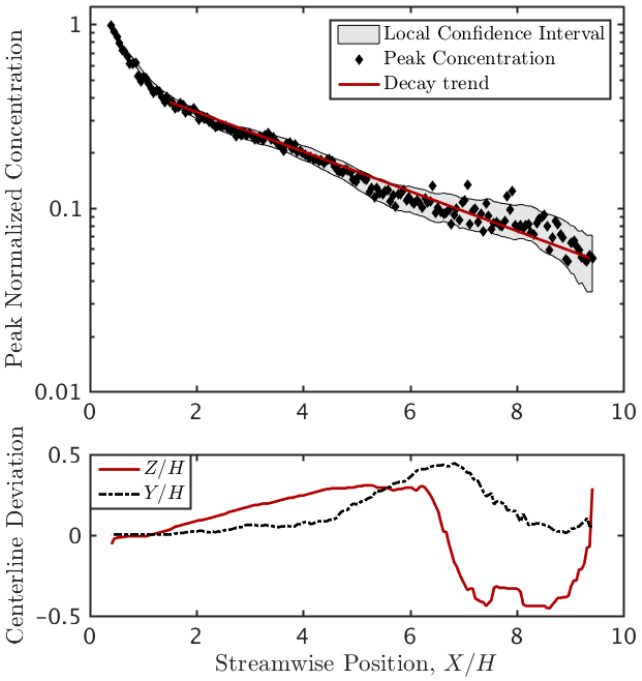

Figure 7. Maximum particle concentration and (Y,Z) position of maximum in channel first passage.

In Fig. 7 only the peak concentration is considered. Figure 7A shows the peak concentration, on a logarithmic scale, as a function of streamwise position X/H. The linear trend after $X/H = 1$ indicates an exponential decay in peak concentration as one moves downstream. The (Y,Z) positions of these peak values are reported in Fig. 7B as a means of tracking the streak's core. The streak makes a full loop around the $+Y$ side of the channel; it first drifts slowly towards the $+Z$ wall, next is rapidly swept to $-Z$ as it interacts with the the $+Y$ ribs, and finally returns to channel center near the bend entry.

Future Work

A calibration experiment is currently being fabricated in which particles can be seeded uniformly and at known concentration

throughout a turbulent, vertically oriented square channel flow. Because clinical MRI machines consist of a horizontal-bore magnet, injection and mixing of particles must be achieved in a short vertical space. Particles are injected into the flow via a shaped, dispersive nozzle and mixed further by 14 rows of pins crossing the channel. The measurement section is constructed from cast acrylic sheets, allowing laser-based measurements to be obtained for validation purposes. The remainder of the channel is built using stereolithography (SLA).

Several goals remain as the focus of the calibration experiment. The first and most critical is to obtain an understanding of how A, the concentration-decay calibration value, behaves in the presence of a turbulent flow. While the integrated particle flux method provided some evidence that flow affects A, the strength of this evidence is limited by the fact that ϕ_v is not known a priori in the SGTIP flow. In addition, the use of a flux-based calibration ignores any potential variation of A *within* a streamwise slice.

By contrast, precise, time-resolved companion measurements of ϕ_v can be made in the calibration rig using an existing, well-validated technique. Such a detailed characterization of the flow will permit an understanding of how R_2^* may be affected by flow velocity or unsteadiness in ϕ_v due to preferential concentration. A range of Reynolds numbers will be tested in the calibration rig in order to vary the velocity, turbulence level, and preferential concentration of the particles. Once any flow effects are well understood, a second goal will be to devise a suitable correction scheme, so that ϕ_v can be obtained without the need for an imperfect, integral-based adjustment.

CONCLUSIONS

A new diagnostic method called MRP was employed, wherein the MRI signal decay rate, R_2^*, was obtained by measuring the MRI signal at several time points (TEs) along the decay curve. Agar gel suspensions of various types of microparticles were imaged using MRP. The calibration constant, A, between R_2^* and particle volume fraction, ϕ_v, agreed well with predictions from the MRI literature, particularly for titanium, bismuth, and graphite particles. Data obtained near a stainless steel particle showed that increasing the diameter and magnetic susceptibility beyond a certain threshold can cause undesireable signal decay at distances larger than the imaging resolution. It was determined that titanium microparticles provide appropriately high signal decay rates at dilute loadings without compromising the spatial resolution of measurements, and are thus an appropriate choice for MRP experiments.

In a separate experiment, a streak of $\sim$30 micron diameter titanium particles was injected at a volume fraction of 1% into the center of turbulent flow at $Re = 20,000$ through the SGTIP model. The exact concentration distribution was not known a priori, so calibration between R_2^* and ϕ_v could only be performed by setting the particle flux through successive streamwise planes to the value known from inlet conditions. The resulting data set is a fully three dimensional map of ϕ_v everywhere in the channel. A quantitative analysis of the particle streak transport and dispersion in the first passage was carried out as an example of the type of analysis permitted by MRP data.

Key questions remain that must be addressed in order to fully validate the MRP method. In particular, the calibration factor A obtained in the SGTIP using the integral flux method was spatially-varying and 15–36% lower than the value predicted by theory (and confirmed in the gel samples). This discrepancy will be the primary focus of an upcoming validation experiment, in which a homogeneous dispersed-phase distribution in a vertical channel flow can be measured using both MRP and existing laser-based techniques. The goal will be to identify, characterize, and design a reliable correction for any flow-related changes to the calibration factor.

REFERENCES

Banko, A. J., Coletti, F., Schiavazzi, D., Elkins, C. J. & Eaton, J. K. 2015 Three-dimensional inspiratory flow in the upper and central human airways. *Experiments in Fluids* **56** (6), 117.

Benson, M. J., Elkins, C. J., Mobley, P. D., Alley, M. T. & Eaton, J. K. 2010 Three-dimensional concentration field measurements in a mixing layer using magnetic resonance imaging. *Experiments in Fluids* **49** (1), 43–55.

Chang, S., Elkins, C., Alley, M., Eaton, J. & Monismitha, S. 2009 Flow inside a coral colony measured using magnetic resonance velocimetry. *Limnology and Oceanography* **54** (5), 1819–1827.

Coletti, F., Borup, D., Elkins, C. & Eaton, J. 2014*a* Measuring Fluid, Scalar, and Particle Transport in Internal Flows Using Medical Imaging. In *17th International Symposium on Applications of Laser Techniques to Fluid Mechanics*.

Coletti, F., Muramatsu, K., Schiavazzi, D., Elkins, C. J. & Eaton, J. K. 2014*b* Fluid flow and scalar transport through porous fins. *Physics of Fluids* **26** (5), 055104.

Dunn, M. G. 2012 Operation of Gas Turbine Engines in an Environment Contaminated with Volcanic Ash. *Journal of Turbomachinery* **134** (5), 051001.

Dunn, M. G., Padova, C., Moller, J. E. & Adams, R. M. 1987 Performance Deterioration of a Turbofan and a Turbojet Engine Upon Exposure to a Dust Environment. *Journal of Engineering for Gas Turbines and Power* **109** (3), 336–343.

Elkins, C. J. & Alley, M. T. 2007 Magnetic resonance velocimetry: applications of magnetic resonance imaging in the measurement of fluid motion. *Experiments in Fluids* **43** (6), 823–858.

Elkins, C. J., Markl, M., Iyengar, A., Wicker, R. & Eaton, John K. 2004 Full-field Velocity and Temperature Measurements Using Magnetic Resonance Imaging in Turbulent Complex Internal Flows. *International Journal of Heat and Fluid Flow* **25** (5), 702–710.

Gu, Hengfeng, Gong, Haijun, Dilip, JJS, Pal, Deepankar, Hicks, Adam, Doak, Heather & Stucker, Brent 2014 Effects of Powder Variation on the Microstructure and Tensile Strength of Ti6Al4V Parts Fabricated by Selective Laser Melting. In *Proceedings of the 25th Solid Freeform Fabrication Symposium.*, pp. 470–483.

Kleinstreuer, C. & Zhang, Z. 2010 Airflow and particle transport in the human respiratory system. *Annual Review of Fluid Mechanics* **42**, 301–334.

Schenck, J. F. 1996 The role of magnetic susceptibility in magnetic resonance imaging: MRI magnetic compatibility of the first and second kinds. *Medical physics* **23** (6), 815–850.

Yablonskiy, D. & Haacke, E. M. 1994 Theory of NMR Signal Behavior in Magnetically Inhomogeneous Tissues: The Static Dephasing Regime. *Magnetic Resonance in Medicine* **32** (6), 749–763.